

Vortex shedding frequency in open-channel lateral cavity

C. Perrot-Minot^{1,†}, E. Mignot², R. Perkins¹, D. Lopez² and N. Riviere²

¹Univ Lyon, Ecole Centrale de Lyon, INSA Lyon, Université Claude Bernard Lyon I, CNRS, Laboratoire de Mécanique des Fluides et d'Acoustique, UMR 5509, 36 Avenue Guy de Collongue, F-69134, Ecully, France

²Univ Lyon, INSA Lyon, Ecole Centrale de Lyon, Université Claude Bernard Lyon I, CNRS, LMFA, UMR 5509, 20 Avenue Albert Einstein, F-69621, Villeurbanne, France

(Received 16 July 2019; revised 29 January 2020; accepted 1 March 2020)

This article aims at predicting the oscillation frequency of open-channel lateral cavities, which are common sheltered zones of riverine environments, and have important ecological impact. Using a theoretical analysis based on an existing model for acoustic cavities and a free-surface lateral cavity experiment, we show that the vortex shedding in the mixing layer between the cavity and the open channel is always constrained by gravity waves even for low Froude numbers ($F < 0.6$). This expands previous results from the literature showing the impact of gravity waves on the vortex shedding frequency for high Froude number ($F > 0.6$). Measurements of the free-surface oscillation and transverse velocity oscillation frequencies reveal a unique frequency along the mixing layer, equal to the free-surface oscillation frequency anywhere in the cavity. Hence, it is shown that the vortex shedding frequency in an open-channel lateral cavity always equals a match between a natural frequency of the cavity and a solution of the feedback model developed herein for low to moderate Froude numbers.

Key words: river dynamics, wave–turbulence interactions, vortex shedding

1. Introduction

Cavities are common features of air or water flows in industrial and environmental applications which can exhibit various shapes, sizes and configurations. Still, they are often simplified as rectangular dead-zones connected through one face to an established one-dimensional flow. Cavities have been extensively studied for acoustic and aeronautic purposes, mostly dealing with aircraft sound generation (Hussain & Zaman 1978; Selfridge, Reiss & Avital 2017). In riverine environments, typical lateral cavities with a free surface are harbours, oxbow lakes or sheltered zones downstream of boulders (Sanjou & Nezu 2013; Jackson, Apte & Haggerty 2015; Sandoval *et al.* 2019). These sheltered zones favour the development of fauna and flora and thus play a major role for ecosystems. Moreover, gravity waves can resonate in such

† Email address for correspondence: clement.perrot-minot@insa-lyon.fr

cavities, producing large oscillations of the free surface, usually called ‘seiche’, and may disable the loading of ships in harbours (Kimura & Hosoda 1997).

For any type of cavity, a mixing layer develops at the interface between the cavity and the main flow. Given the strong velocity gradient across the mixing layer, Kelvin–Helmholtz instability develops into coherent vortices, generated in the upstream region of the mixing layer and advected downstream (Raupach, Finnigan & Brunet 1996; Charru 2007). Rockwell & Knisely (1978) reported that in such a bounded mixing layer, vortices are highly coherent, which differs from what is typically encountered in convective mixing layers (Godreche 1998). Here the coherency is maintained all along the mixing layer, meaning no vortex pairing occurs. Consequently, the frequencies of vortex shedding (at the upstream edge) and impingement (at the downstream edge) are equal, and are referred to as ‘cavity frequencies’ in what follows.

In a riverine environment, the mixing layer governs momentum (Mignot, Cai & Riviere 2019) and mass (Sanjou & Nezu 2013) exchanges between the cavity and the main stream as well as the free-surface oscillation (Meile, Boillat & Schleiss 2011). Knowledge of the cavity frequency is thus crucial for the management of cavity flows. Cavities without a free surface, where only pressure waves travel, are defined as ‘acoustic cavities’. Their behaviour is very similar to that of open-channel cavities where gravity waves propagate with a much higher energy. Despite their similarities, they exhibit key differences.

In acoustics, the cavity frequency depends on the Mach number ($M = U/c_p$), which compares the flow velocity U to the pressure wave celerity c_p . For low Mach numbers ($M < 0.2$), the cavity frequency is governed by the natural frequency of the cavity, whereas for high Mach numbers ($M > 0.2$), it is governed by a feedback loop between vortices and pressure waves (Rossiter 1964). Moreover, several frequencies can coexist at the same time, for a fixed Mach number (Larcheveque *et al.* 2003).

In open-channel cavities, Wolfinger, Ozen & Rockwell (2012) recently measured the evolution of this frequency with the Froude number of the main stream. The Froude number, $F = U/c$, compares the flow velocity U to the gravity wave celerity c , similar to the Mach number for acoustic cavities. In this case though, the vortex shedding frequency is ‘locked on’ a natural frequency of the cavity and the frequency remains constant for high Froude numbers ($0.6 < F < 1$). For lower Froude numbers ($F < 0.6$), the frequency increases with the Froude number. Moreover, Wolfinger *et al.* (2012) reveal that only one frequency is observed for a given flow (with sometimes its first harmonic). These results exhibit an opposite behaviour between acoustic and open-channel cavities. The authors then proposed an experimental linear trend of the oscillation frequency as a function of the Froude number. Even though a feedback loop was mentioned for a riverine environment (Tsubaki & Fujita 2006), no analytical prediction of the oscillation frequency has been proposed to the best of our knowledge. Hence, it remains unknown if the frequencies measured by Wolfinger *et al.* (2012) correspond to a feedback loop similar to the one measured and modelled in acoustic cavities. The major difference lies in the different types of feedback waves: pressure waves for acoustic cavities and gravity waves in open channels.

The aim of the present work is to take advantage of the existing knowledge available in the area of acoustic cavities to explain and model the surface oscillation and vortex frequencies in open-channel cavities. Section 2 recalls the theory for the feedback model applied to acoustic cavities and proposes an adaptation for open-channel conditions. Section 3 introduces the experimental set-up used for the validation as well as the measurement techniques employed herein. Finally § 4 presents the capabilities of the model in predicting the cavity frequency for open-channel cavities, followed by a conclusion in § 5.

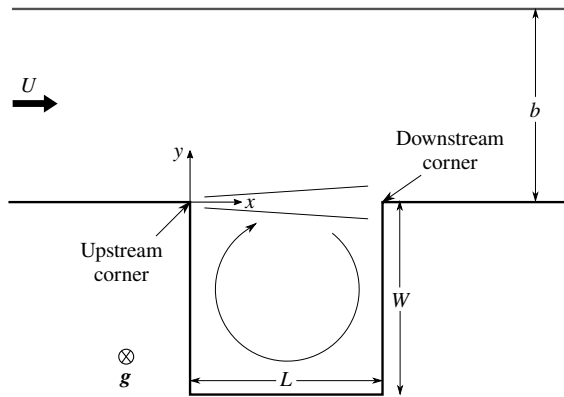


FIGURE 1. Experimental set-up (top view).

2. Theoretical model for vortex frequency

2.1. Model for frequency prediction in acoustics

As introduced in § 1, the analytical model predicting the cavity frequency in acoustics relies on the natural frequency for low Mach numbers and on the feedback loop in the mixing layer for high Mach numbers.

The natural frequency of an acoustic cavity can be computed by simplifying it as a rectangular enclosure with fluid at rest (Plumbee, Gibson & Lassiter 1962). This frequency is ‘natural’ as it is an intrinsic property of the cavity, and does not depend on the adjacent flow. Cavity-type oscillations, induced by compressibility effects, can also be computed using the Helmholtz resonator theory.

For the feedback loop, the model considers the following events. As a vortex is shed (near the upstream corner of the cavity, denoted by subscript v , with a phase Φ_v), it is advected by the flow and impinges the downstream corner. There, it generates a local pressure variation (following the Bernoulli principle) inducing a pressure wave (denoted by subscript p , with a phase Φ_p) with the same frequency as that of the vortex shedding, which propagates in every direction, including upwards, i.e. towards the upstream corner of the cavity. The model assumes that the selected frequency is the one that fulfils the resonant conditions. This implies that the phase difference $\Delta\Phi = \Phi_v - \Phi_p$, where v and p refer to vortex and pressure waves (see figure 1) at the upstream corner, satisfies

$$\Delta\Phi(x=0) = 2N\pi, \tag{2.1}$$

with N being an integer ($N = 1, 2, 3, \dots$). Using the definition of the wavelength $\lambda = c/f$, with c the celerity of waves and f their frequency, this reads

$$N = \frac{L}{\lambda_v} + \frac{L}{\lambda_p}. \tag{2.2}$$

Integer N can be seen as the number of vortices plus pressure wave wavelengths along the cavity–main flow interface ($x = 0$ to L). Using $f = c_v/\lambda_v = c_p/\lambda_p$, this reads

$$N = \frac{Lf}{c_v} + \frac{Lf}{c_p}, \tag{2.3}$$

or alternatively, introducing the Strouhal number

$$St = \frac{fL}{U} = \frac{N}{\frac{U}{c_v} + \frac{U}{c_p}}, \quad (2.4)$$

with U the velocity of the main stream. The value of the ratio $R_v = c_v/U$ is usually measured experimentally, and R_v has been reported as ranging between 0.35 (East 1966) and 0.625 (Rowley *et al.* 2006). Rossiter (1964) states that $R_v = 0.57$, which is the standard value used in the literature.

For a given flow configuration, this model allows an infinity of solutions, with $N = 1, 2, 3$, etc. Rossiter (1964) and subsequent authors compared the frequency predicted by this model with experimental data and noticed a systematic shift. Most of them thus introduce a correction factor, ΔN with $N' = N + \Delta N$, attributed to 'a constant phase lag corresponding to a time delay between the vortex arrival at the impingement corner and the emission of the acoustic pulse' (Gloefert 2009). The corrected model then reads

$$\frac{fL}{U} = \frac{N + \Delta N}{\frac{1}{R_v} + M}. \quad (2.5)$$

Empirical values for ΔN , proposed by successive authors, exhibit a large variation, from $\Delta N = -0.58$ (Rossiter 1964) to $\Delta N = 0.5$ (Sarohia 1977). A global three-dimensional stability analysis of the mixing layer (Bilanin & Covert 1973; Alvarez, Kerschen & Tumin 2004), injecting the resonant condition, leads to a similar result. Note that the celerity of the pressure wave does not take into account the local flow velocity as it is supposed to travel in the cavity, where the mean velocity is negligible. The fact that the model applies to supersonic flows ($M > 1$) supports this hypothesis, as the wave could not propagate upstream otherwise.

2.2. Transposition to open-channel configurations

We expect that the oscillation frequency of open-channel cavities is governed by the same two phenomena. They are transposed to the open-channel configuration in the following subsections.

2.2.1. Natural frequencies of open-channel cavities

The natural modes of a closed rectangular water volume at rest were initially introduced by Lamb (1945) and recently reviewed by Rabinovitch (2009). These modes can be aligned with one or both cavity axes x and y (see table 1). The corresponding frequencies are denoted $f_{n_x n_y}$ with n_x and n_y the number of nodes along axes x and y , respectively. In a rectangular basin of dimensions l_x (along axis x) and l_y (along axis y), the natural frequencies then read

$$f_{n_x n_y} = \frac{c}{2} \left[\left(\frac{n_x}{l_x} \right)^2 + \left(\frac{n_y}{l_y} \right)^2 \right]^{1/2}, \quad (2.6)$$

with c the celerity of gravity waves in still water (Stocker 1957):

$$c = \frac{g}{2\pi f} \tanh \frac{2\pi \bar{h} f}{c}, \quad (2.7)$$

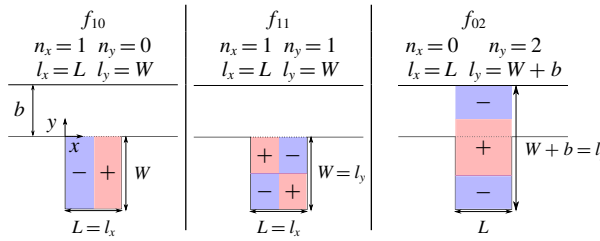


TABLE 1. Three amongst the most common natural frequencies of a rectangular open-channel cavity.

where \bar{h} is the time-averaged water depth in the cavity and f the frequency of the gravity wave. Note that this expression can reduce to the classical Merian (1828) expression for shallow conditions ($\lambda \gg \bar{h}$) if $n_x = 1, n_y = 0$ and c is simplified to $c = \sqrt{g\bar{h}}$. Following the notation of Wolfinger *et al.* (2012) and Tuna, Tinar & Rockwell (2013), f can be normalized by $f_{10} = c/2L$, the natural frequency of the cavity corresponding to the first longitudinal mode (along x) with one node (see table 1):

$$\frac{f_{n_x n_y}}{f_{10}} = \left[n_x^2 + \left(n_y \frac{l_x}{l_y} \right)^2 \right]^{1/2}. \tag{2.8}$$

Table 1 plots schematic views of three observed modes of the cavity and indicates the link between l_x, l_y and W, b, L that depends on the cavity mode considered.

2.2.2. Feedback model adapted to open-channel cavities

When applied to open-channel lateral cavities, the feedback model relies on the same processes as for acoustic cavities with a gravity wave instead of a pressure wave. In the axis frame linked to the cavity (see figure 1), this gravity wave travels upstream at a celerity c . As for the acoustic model, we assume here that: (1) both vortex and gravity waves are periodic with the same frequency f and (2) they are in phase at both corners so that equations (2.3) and (2.5) still hold:

$$N = \frac{Lf}{c_v} + \frac{Lf}{c}. \tag{2.9}$$

Following the same normalization as for equation (2.8) and including the correction factor, the feedback frequency reads

$$\frac{f}{f_{10}} = \frac{2F(N + \Delta N)}{\frac{1}{R_v} + F}. \tag{2.10}$$

Again, equation (2.10) produces an infinity of solutions.

3. Experiments

3.1. Experimental campaign

Measurements aiming at validating the analytical model were performed at INSA-Universite de Lyon in a set-up similar to that used by Mignot *et al.* (2016). It consists

of a 4.80 m long and $b = 30$ cm wide open channel connected at mid-length to an adjacent rectangular lateral cavity. The channel and the cavity are horizontal, of rectangular section with glass bottom and sidewalls, with no step at the connection. At the channel inlet, the water overflows from the tank to the upstream branch of the channel through a converging section. Moreover, honeycomb meshes straighten the flow. At the outlet, a sharp crested weir adjusts the time-averaged water depth $\bar{h} = 5.8$ cm at the connection with the cavity. The flow finally recirculates in a closed loop and the corresponding flow rate is measured by an electromagnetic flow meter (ProMag50, Endress Hauser) with an uncertainty of ± 0.05 l s⁻¹. The length of the cavity (in the direction parallel to the channel) is fixed at $L = 0.3$ m and its width $W = 0.5$ m.

According to a dimensional analysis, the oscillation frequency depends on three parameters: W/L , b/L and F . The strategy proposed herein is to keep W/L and b/L constant while varying the Froude number from $F = 0.33$ to 0.65, corresponding to the range of Froude numbers for which Wolfinger *et al.* (2012) reported an increasing cavity frequency (for $0.3 < F < 0.6$) followed by a lock-on regime (i.e. a linearly constant oscillation frequency value for $0.6 < F < 0.85$). Unfortunately, due to experimental constraints, the Froude number could not be increased beyond 0.65 for the present experimental device. In order to avoid any hysteresis effect, each configuration is initiated with the cavity flow at rest and measurements start after the water-level oscillations at the downstream corner reach a steady state.

3.2. Measurement methods

Three types of measurements are considered herein, using three different methods. The oscillation of the free surface near the downstream corner of the interface (figure 1) is measured using an ultrasonic probe, UNDK 20I6912 S35A from Baumer Electric AG (resolution $\delta h \leq 0.3$ mm), with a sampling frequency equal to 200 Hz. Data are recorded during 10 min. Secondly, the two-dimensional horizontal velocity field, and associated vortex dynamics, in the region surrounding the interface is measured using particle image velocimetry. A 1 mm thick horizontal laser sheet is used to illuminate a horizontal plane across the mixing layer at $z/\bar{h} = 0.8$. The images are recorded from underneath the flume, using an AV Manta G-235B camera, 1936×1216 pixels with a spatial resolution of 0.3 mm per pixel. For each flow configuration, 33.3 s are recorded at a sampling frequency of 60 fps (2000 images). Finally, the two-dimensional free-surface deformation is measured using a fringe pattern projection method adapted from Takeda, Ina & Kobayashi (1981) and Przadka *et al.* (2011). A video projector, located 1.5 m above the free surface, projects vertically (downward) on the free surface a known fringe pattern image. The oscillation of the free surface then deforms the pattern so that the water depth displacement is computed at each pixel on each image by extracting the phase difference between the deformed and reference patterns. The post-processing finally applied is adapted from Aubourg (2006). In the end, for each flow configuration, the frequency of vortex shedding and free-surface oscillation is measured using three different methods, on three different days as these measurement techniques could not be applied simultaneously. The fair agreement between these frequencies gives confidence in the reproducibility and precision of the methods.

4. Results

4.1. Determination of R_v in open-channel cavities

The feedback model (2.10) requires one to estimate $R_v = c_v/U$. The evolution of R_v with the Froude number is plotted in figure 2(b), c_v being obtained by averaging the

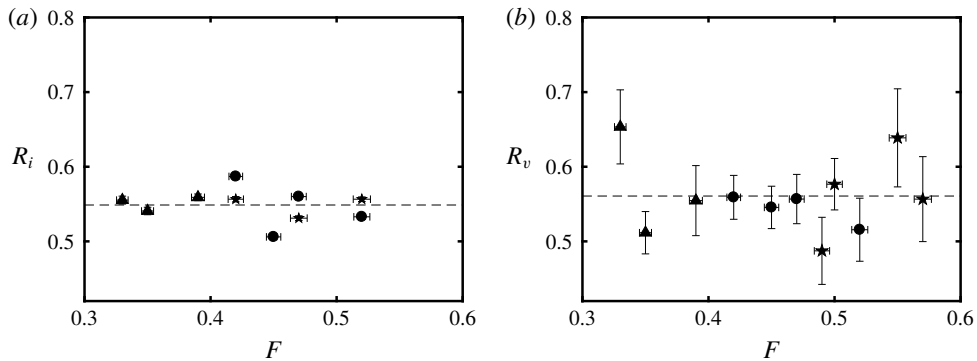


FIGURE 2. Dependence of the mixing layer dynamics on Froude number. (a) Ratio of interface flow velocity to bulk velocity with respect to Froude number. (b) Ratio of vortex velocity to bulk velocity with respect to Froude number.

travelling time of 40 consecutive vortices along the interface of the cavity, using the methodology proposed by Mignot *et al.* (2016). Ratio R_v appears to remain constant with F : $R_v = 0.56$ is in good agreement with the value reported by Rossiter (1964) ($R_v = 0.57$) for acoustic cavities.

4.2. Experimental validation of the model

Figure 3(a) plots the first three solutions of the feedback model (2.10) as solid lines, for $N = 1, 2$ and 3, here without correction ($\Delta N = 0$), as well as data from Wolfinger *et al.* (2012) as red squares. It shows that these data closely match the mode $N = 2$ of the feedback model, suggesting that the apparently linear trend observed by Wolfinger *et al.* (2012) for $F < 0.6$ corresponds actually to the second feedback mode of the mixing layer. Figure 3(a) additionally plots the natural frequencies of the cavity, equation (2.8), as dashed horizontal lines. As already observed by Kegerise (1999), feedback and natural frequencies exhibit several matches for different Froude numbers. The selected frequencies are thus expected to fit, at best, these matches.

Free-surface oscillation frequencies from ultrasound measurements at the impingement corner are finally included in figure 3(a) (green symbols) for Froude numbers ranging from 0.3 to 0.65. While the frequencies measured by Wolfinger *et al.* (2012) linearly increase with the Froude number for $F < 0.6$, the present frequencies exhibit a different trend, divided in three ranges of Froude numbers.

First, for $0.33 < F < 0.4$, the measured frequencies remain about constant at a value corresponding to mode f_{02} and close to the feedback mode $N = 2$ (2.10). To check the free-surface oscillation mode, figure 3(b) plots a snapshot of the free-surface deformation, obtained by fringe pattern projection, for the flow configuration with $F = 0.35$. It reveals two wave crests along the cavity ($y = -W$) and main channel ($y = b$) walls, a trough at mid-length and two nodes depicted as white lines aligned along the x axis. This confirms the natural mode associated with f_{02} (table 1). Note that a similar pattern is retrieved for all configurations with $F < 0.4$, so that the corresponding symbols in figure 3(a) are plotted as triangles. The plateau reveals that the cavity oscillation frequency is locked on a natural mode of the cavity. Furthermore, it is possible to estimate the experimental value of N , denoted N_e , using (2.9) (where f , U_i and c_v are measured as described above): $N_e = [2.08, 2.32]$ agrees fairly well with the expected mode $N = 2$ giving confidence in the validity of the feedback model.

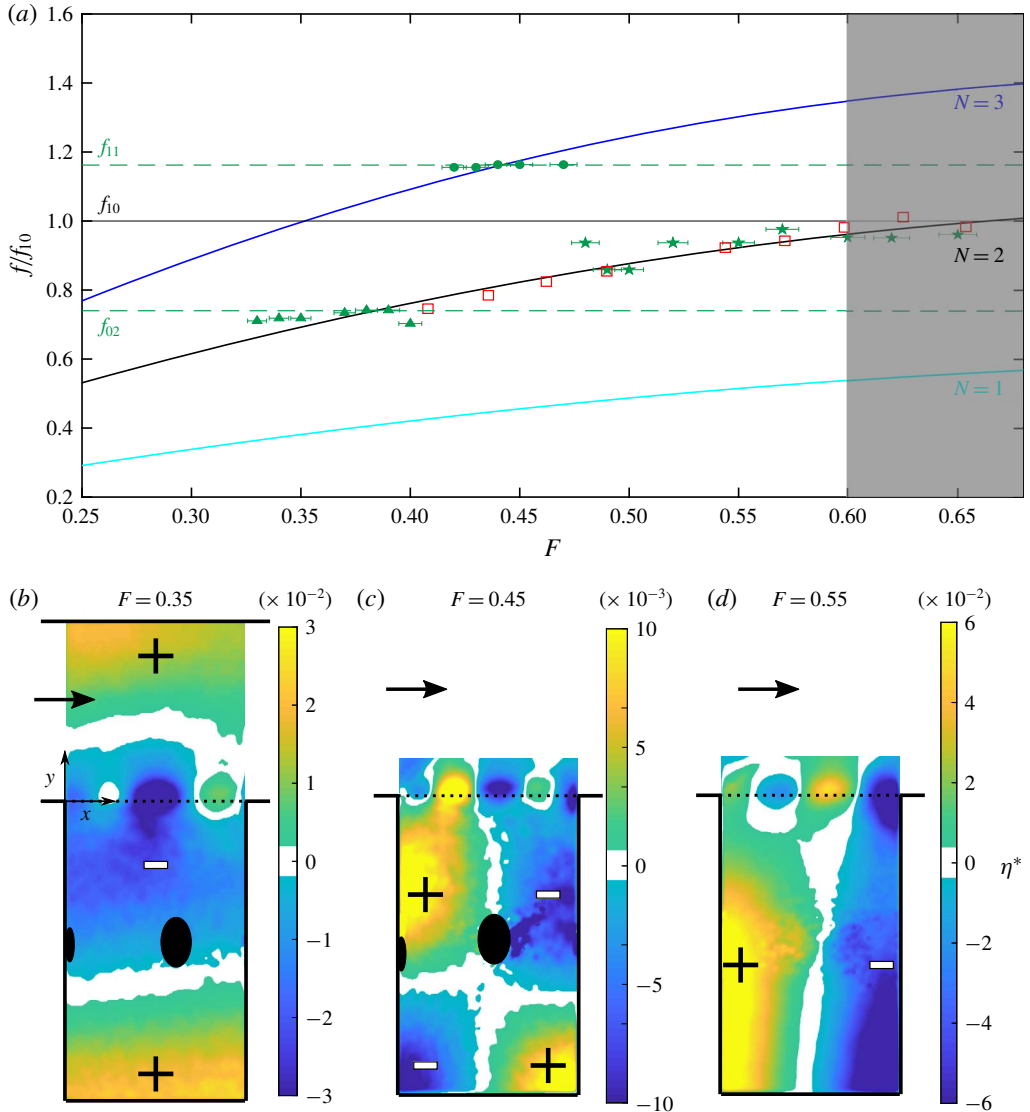


FIGURE 3. Experimental validation of the feedback model. (a) Evolution of normalized frequency of free-surface oscillation with respect to Froude number. Red squares are data from Wolfinger *et al.* (2012). Solid lines are the three first modes ($N = 1, 2, 3$) of the model with $\Delta N = 0$ obtained as best fitting. Dashed lines correspond to natural frequencies of the cavity. (b–d) Snapshots of the normalized free-surface oscillation $\eta^* = \eta/U^2/2g$; black zones are measurement noise due to direct light reflection.

Similarly, for $0.4 < F < 0.48$, the frequencies are close to f_{11} and to the feedback mode $N = 3$ (2.10). The snapshot of the free-surface deformation for $F = 0.45$ (figure 3c) reveals a chessboard pattern, with two crests: one at the upstream corner of the cavity and one at the opposite corner ($x = L, y = -W$); and two troughs: one at the downstream corner of the interface and the other at the opposite corner ($x = 0, y = -W$). The two nodes are aligned along x and y axes. This f_{11} mode is retrieved for

all configurations with $0.4 < F < 0.48$, and the corresponding symbols in figure 3(a) are plotted as circles. For this second plateau, the cavity oscillation frequency is locked on a second natural mode of the cavity. Moreover, $N_e = [2.80, 3.16]$ agrees with the expected feedback mode $N = 3$.

Finally, for $0.48 < F < 0.65$, frequencies are close to feedback mode $N = 3$ and near the natural mode f_{10} . This third plateau corresponds to a third lock-on, similar to that reported by Wolfinger *et al.* (2012) but starting at a lower value of Froude number: namely $F \approx 0.48$ instead of $F \approx 0.6$, reported by those authors. The snapshot of the free-surface deformation for $F = 0.55$ (figure 3d) shows one crest and one trough along the lateral walls of the cavity and one node in between. This confirms that the free-surface deformation corresponds to f_{10} mode. A similar tendency is retrieved for all configurations with $0.48 < F < 0.6$ and the symbols are plotted as stars in figure 3(a). Also, $N_e = [1.99, 2.03]$ agrees with the expected feedback mode $N = 2$.

To summarize, the peak frequencies of the cavity oscillation are distributed among three lock-on plateaus, which correspond to close matches between a feedback mode in the mixing layer (but with less agreement for the third plateau) and a natural mode of the cavity for the free-surface deformation. Still, other matches between feedback modes (2.10) and natural modes (2.8) could have been selected for several flow configurations. For instance, natural mode f_{10} and feedback mode $N = 3$ match for $F \approx 0.35$ (figure 3a) while the observed mode corresponds to a match of f_{02} and $N = 2$. The mode selection in this case is thus still an open question at this stage.

5. Conclusion

The present paper deals with open-channel cavity flows for incoming Froude numbers ranging from 0.33 to 0.65. It is shown that the processes governing vortex shedding substantially differ from those of classical free mixing layers. This difference is due to the interaction of the vortex shedding with the gravity waves of two different kinds that are encountered in the flow. Waves of the first kind are standing waves. They correspond to the natural modes of the cavity and their frequencies are well predicted by classical equations. Waves of the second kind are the feedback gravity waves. They propagate against the current and their frequencies are well predicted by the so-called feedback model developed in this work, taking inspiration from acoustic cavity models. In this study, the interactions are always observed jointly with the two types of waves. In other words, the frequency of the vortex shedding always matches with a common solution to the two models. However, for a given Froude number, several common solutions exist.

The selection of the resonant mode may result from the different values of damping of each available natural mode of the cavity. An attempt to estimate these damping rates could be made through a numerical stability analysis. Another process that selects the resonant mode could be another feedback process (other than the Rossiter modes), related to the motion of vortices along the recirculation cell inside the cavity. This cell can indeed trap vortices near the impingement edge of the cavity, make them rotate along the cavity walls and reintroduce them at the upstream edge (Mignot & Brevis 2019), where they could interact with the vortex shedding process. The selection of the actual resonant mode of the cavity is thus still an open question, which should be addressed in future works.

Acknowledgements

This work was performed under the framework of PHC-Tournesol 2018-40633YJ. The authors are grateful to L. Engelen and T. De Mulder from the University of Ghent for fruitful discussions.

Declaration of interests

The authors report no conflict of interest.

REFERENCES

- ALVAREZ, J. O., KERSCHEN, E. J. & TUMIN, A. 2004 A theoretical model for cavity acoustic resonances in subsonic flow. In *10th AIAA/CEAS Aeroacoustics Conference*, p. 2845. American institute of Aeronautics & Astronautics.
- AUBOURG, Q. 2006 Etude experimentale de la turbulence d'ondes a la surface d'un fluide. la theorie de la turbulence faible à l'épreuve de la realite pour les ondes de capillarite et gravite. PhD thesis, Ecole Doctorale Ingenierie Materiaux, Mecanique, Environnement, Energetique, Procedes, Production. Universite Grenoble Alpes, Grenoble.
- BILANIN, A. J. & COVERT, E. 1973 Estimation of possible excitation frequencies for shallow rectangular cavities. *AIAA J.* **11** (3), 347–351.
- CHARRU, F. 2007 *Instabilités Hydrodynamiques*. Savoirs Actuels.
- EAST, L. F. 1966 Aerodynamically induced resonance in rectangular cavities. *J. Sound Vib.* **3** (3), 277–287.
- GLOEFERT, X. 2009 Cavity noise.
- GODRECHE, C. 1998 *Hydrodynamics and Nonlinear Instabilities*. Cambridge University Press.
- HO, C. M. & NOSSEIR, N. S. 1981 Dynamics of an impinging jet. Part 1. The feedback phenomenon. *J. Fluid Mech.* **105**, 119–142.
- HUSSAIN, A. K. M. F. & ZAMAN, K. B. M. Q. 1978 The free shear layer tone phenomenon and probe interference. *J. Fluid Mech.* **87**, 349–383.
- JACKSON, T. R., APTE, S. V. & HAGGERTY, R. 2015 Flow structure and mean residence times of lateral cavities in open channel flows: influence of bed roughness and shape. *Environ. Fluid Mech.* **15**, 1069–1100.
- KEGERISE, M. A. 1999 An experimental investigation of flow-induced cavity oscillations. PhD thesis, Syracuse University.
- KIMURA, I. & HOSODA, T. 1997 Fundamental properties of flows in open channels with dead zone. *J. Hydraul. Engng ASCE* **123** (2), 98–127.
- LAMB, H. 1945 *Hydrodynamics*. Cambridge University Press.
- LARCHEVEQUE, L., SAGAUT, P., MARY, I., LABBE, O. & COMTE, P. 2003 Large-eddy simulation of a compressible flow past a deep cavity. *Phys. Fluids*.
- MEILE, T., BOILLAT, J.-L. & SCHLEISS, A. J. 2011 Water-surface oscillations in channels with aximmetric cavities. *J. Hydraul. Res.* **49** (1), 73–81.
- MERIAN, J. R. 1828 Ueber die bewegung tropfbarer flüssigkeiten in gefassen [on the motion of drippable liquids in containers]. PhD thesis, Basle.
- MIGNOT, E. & BREVIS, W. 2019 Coherent turbulent structures within open-channel lateral cavities. *J. Hydraul. Engng ASCE* **146** (2).
- MIGNOT, E., CAI, W., LAUNAY, G. & ESCAURIAZA, C. 2016 Coherent turbulent structures at the mixing-interface of a square open-channel cavity. *Phys. Fluids* **28**, 16.
- MIGNOT, E., CAI, W. & RIVIERE, N. 2019 Analysis of the transitions between flow patterns in open-channel lateral cavities with increasing aspect ratio. *Environ. Fluid Mech.* **19** (1), 231–253.
- PLUMBEE, H. F., GIBSON, J. S. & LASSITER, L. W. 1962 A theoretical and experimental investigation of the acoustic response of cavities in an aerodynamic flow. *Tech. Rep.* US Air Force.
- PRZADKA, A., CABANE, B., PAGNEUX, V., MAUREL, A. & PETITJEANS, P. 2011 Fourier transform profilometry for water waves: how to achieve clean water attenuation with diffusive reflection at the water surface. *Exp. Fluids* **52**, 519–527.
- RABINOVITCH, A. B. 2009 *Seiches and Harbor Oscillations*, chap. 9. World Scientific Publisher.
- RAUPACH, M. R., FINNIGAN, J. J. & BRUNET, Y. 1996 *Coherent Eddies and Turbulence in Vegetation Canopies: the Mixing Layer Analogy*. Kluwer Academic Publishers.

- ROCKWELL, D. & KNISELY, C. 1978 The organized nature of flow impingement upon a corner. *J. Fluid Mech.* **93**, 413–432.
- ROSSITER, J. E. 1964 Wind-tunnel experiments on the flow over rectangular cavities at subsonic and transonic speeds. *Tech. Rep.* Aeronautical Research Council Reports and Memoranda.
- ROWLEY, C. W., WILLIAMS, D. R., COLONIUS, T., MURRAY, R. M. & MACMYNOWSKI, D. G. 2006 Linear models for control of cavity flow oscillations. *J. Fluid Mech.* **547**, 317–330.
- SANDOVAL, J., MIGNOT, E., MAO, L., BOLSTER, D. & ESCAURIAZA, C. 2019 Field and numerical investigation of transport mechanisms in a surface storage zone. *J. Geophys. Res.* **124** (4), 938–959.
- SANJOU, M. & NEZU, I. 2013 Hydrodynamic characteristics and related mass-transfer properties in open-channel flows with rectangular embayment zone. *Environ. Fluid Mech.* **13**, 527–555.
- SAROHIA, V. 1977 Experimental investigation of oscillations in flows over shallow cavities. *AIAA J.* **15** (7), 984–991.
- SELFRIDGE, R., REISS, J. D. & AVITAL, E. J. 2017 Physically derived synthesis model of a cavity tone. In *Proceedings of the 20th International Conference on Digital Audio Effects*, pp. 5–9.
- STOCKER, J. J. 1957 *Water Waves, The Mathematical Theory with Applications*. Interscience Publishers.
- TAKEDA, M., INA, H. & KOBAYASHI, S. 1981 Fourier-transform method of fringe-pattern analysis for computer-based topography and interferometry. *J. Opt. Soc.* **72** (1), 156–160.
- TSUBAKI, R. & FUJITA, I. 2006 Surface oscillation in flow past a side cavity using stereoscopic measurement and pod. *J. Hydrosoci. Hydraul. Engng* **24** (2), 41–51.
- TUNA, B. A., TINAR, E. & ROCKWELL, D. 2013 Shallow flow past a cavity: globally coupled oscillations as a function of depth. *Exp. Fluids* **54**, 20.
- WOLFINGER, M., OZEN, C. A. & ROCKWELL, D. 2012 Shallow flow past a cavity: coupling with a standing gravity wave. *Phys. Fluids* **24**, 16.